PHILOSOPHICAL TRANSACTIONS OF THE ROYAL SOCIETY A

rsta.royalsocietypublishing.org

Research

Cite this article: Verschueren N, Bortolozzo U, Clerc MG, Residori S. 2014 Chaoticon: localized pattern with permanent dynamics. *Phil. Trans. R. Soc. A* **372**: 20140011. http://dx.doi.org/10.1098/rsta.2014.0011

One contribution of 19 to a Theme Issue 'Localized structures in dissipative media: from optics to plant ecology'.

Subject Areas:
optics, complexity, mathematical physics

Keywords:
pattern formation, localized structures, spatio-temporal chaos

Author for correspondence:
Marcel G. Clerc
e-mail: marcel@dfi.uchile.cl

Chaoticon: localized pattern with permanent dynamics

N. Verschueren[1], U. Bortolozzo[2], M. G. Clerc[1] and S. Residori[2]

[1]Departamento de Física, FCFM, Universidad de Chile, Casilla 487-3, Santiago, Chile
[2]INLN, Université de Nice-Sophia Antipolis, CNRS, 1361 route des Lucioles, 06560 Valbonne, France

An analytical mechanism that support localized spatio-temporal chaos is provided. We consider a simple model—*the Nagumo Kuramoto model*—which contains the crucial ingredients for observing localized spatio-temporal chaos, namely, the spatio-temporal chaotic pattern and its coexistence with a uniform state. This model allows us to unveil the front dynamics and to show that it can be described by a chaotic motor corresponding to the deterministic counterpart of a Brownian motor. Front interaction is identified as the mechanism at the origin of the localized spatio-temporal chaotic structures.

1. Introduction

Macroscopic systems under the injection and dissipation of energy and momenta are characterized by exhibiting *self-structuring phenomena* [1–3]. In most of these systems, it has been observed the emergence of localized states [4–6], which, although being spatially extended, exhibit properties associated with particle-like states, such as position, width and charges. In one-dimensional extended systems, localized states can be described as spatial trajectories that connect one steady state with itself, which means they are homoclinic orbits from the point of view of dynamical systems [7]. Consequently, one could imagine localized states of different types supported by different equilibrium states, for example, a uniform state over a pattern [8,9], a pattern over a pattern [10], an oscillatory state over a uniform one [11] or a wave over a uniform state [12] or an oscillatory state [13], to mention a few. For localized oscillatory states, dissipative breathers, it has been shown that if one

Royal Society Publishing

increases the intensity of the forcing, the amplitude of the breather undergoes a double-period route to chaos, hence realizing a low-dimensional localized chaotic state [11].

Recently, we have reported localized states characterized by spatio-temporal chaotic dynamics developing over a uniform state [14]. We have termed these states as chaoticons. Furthermore, we have provided evidence of spatio-temporal chaotic localized structures in a liquid crystal light valve (LCLV) experiment with optical feedback.

The purpose of this paper is to investigate and establish the analytical mechanism of localized spatio-temporal chaotic states in one-dimensional extended systems. The Nagumo Kuramoto model is considered, which contains the essential ingredients for observing localized spatio-temporal chaos: coexistence of spatio-temporal chaotic patterns with a uniform state. The main advantage of this model is that one can control the characteristic intensity of the spatio-temporal chaos. This model allows us to unveil the front dynamics, which is characterized by a chaotic motor, and the front interaction mechanism as the origin of the localized spatio-temporal chaotic structures.

2. Experimental observation of chaoticons in liquid crystal light valve with optical feedback

An LCLV experiment is composed of a nematic liquid crystal (LC) film sandwiched in between a glass and a photoconductive plate over which a dielectric mirror is deposited (for details, see e.g. the review by Residori [15]). The LC film has a planar aligned nematic director $\boldsymbol{n}$ parallel to the walls, with a thickness $d = 15\,\mu\text{m}$. The nematic LC is LC-654, produced by NIOPIK, with a dielectric anisotropy $\Delta\varepsilon \equiv \varepsilon_{\parallel} - \varepsilon_{\perp} = 10.7$ and optical birefringence, $\Delta n \equiv n_{\parallel} - n_{\perp} = 0.2$, where $\varepsilon_{\parallel}$ and $\varepsilon_{\perp}$ are the dielectric permittivities $\parallel$ and $\perp$ to $\boldsymbol{n}$, respectively, and $n_{\parallel}$, $n_{\perp}$ are the extraordinary ($\parallel$ to $\boldsymbol{n}$) and ordinary ($\perp$ to $\boldsymbol{n}$) refractive indices. Transparent electrodes over the glass plates permit the application of an electrical voltage across the LC layer, which allows applying a reference voltage V_0 without feedback. The photoconductor behaves like a variable resistance, decreasing for increasing illumination. The feedback is obtained by sending back onto the photoconductor the light which has passed through the LC layer and has been reflected by the dielectric mirror [15]. This light beam experiences a phase shift which depends on the LC reorientation and, on its turn, modulates the effective voltage that locally applies to the LC layer. The optical free propagation length in the feedback loop is fixed to $L = -4.0\,\text{cm}$.

For a fixed voltage V_0, by increasing the laser intensity the system exhibits a bistability between a spatio-temporal complex pattern and a homogeneous state [14]. Close this coexistence region, one expects to observe a localized spatio-temporal states [7,9]. Figure 1*a* illustrates an experimentally observed chaoticon state. The left panel is the spatio-temporal evolution of the light intensity, represented through an iso-surface. The top right panel show a localized structure at a given instant time, whereas the bottom right panel is a spatio-temporal diagram of a given linear section, which illustrates an intricate localized state. When we increase or decrease the laser intensity the localized structure becomes unstable giving rise to a front propagation between a uniform state and a complex spatio-temporal one. Figure 1*b* shows the observed front propagation dynamics. Depending on the region of parameters one of the two states becomes more favourable and invades the other one, and inversely. The deep understanding of fronts developing from a spatio-temporal chaotic state over an uniform one, and the consequent generation of dynamically interlaced localized structures, are open problems. In the next section, we face this complex problem by means of a simple dynamical model.

3. The Nagumo–Kuramoto model

As we have mentioned before, the main ingredient for the appearance of chaoticon states is the coexistence of a spatio-temporal chaotic pattern with a uniform state. Figure 2*a* illustrates

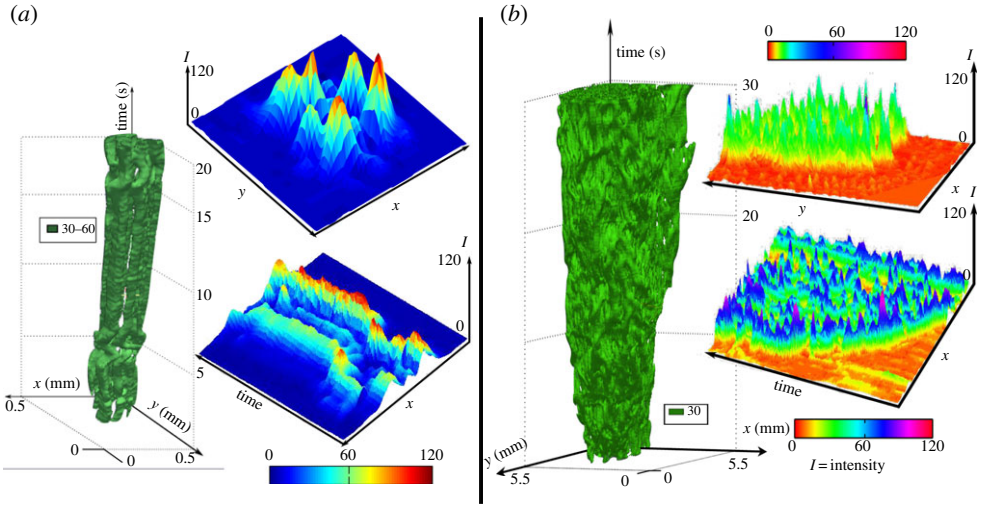

Figure 1. Experimental observations of localized patterns with permanent dynamic and front propagation in the LCLV with optical feedback. (*a*) Example of localized structure with permanent dynamics (chaoticon). The left panel is a spatio-temporal iso-surface diagram of the light intensity in arbitrary units, the top right panel is a surface plot of the light intensity at given time, and the button right panel is a spatio-temporal diagram of a linear section of the light intensity. The input intensity is $I = 2.5$ mW cm^{-2}. (*b*) Front propagation between a spatio-temporal complex and uniform state. The left panel is a spatio-temporal iso-surface diagram of the light intensity in arbitrary units, the top right panel is a surface plot of the light intensity at given time, and the button right panel is a spatio-temporal diagram of a linear section of the light intensity. The input intensity is $I = 2.7$ mW cm^{-2}. (Online version in colour.)

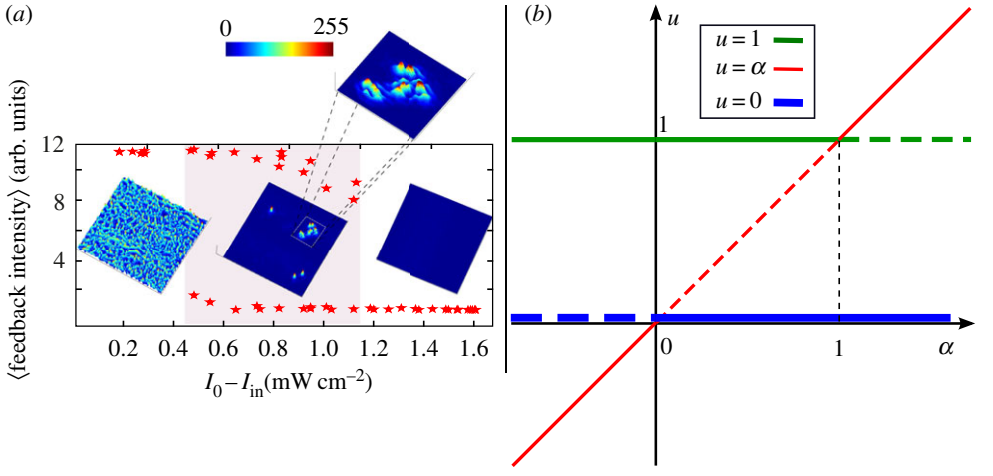

Figure 2. (*a*) Bifurcation diagram of the LCLV experiment, the stars show the average intensity reaching at the camera as the laser intensity is changed. The insets correspond to snapshots of the experiment in each of the three representative zones. (*b*) Bifurcation diagram of the Nagumo–Kuramoto (3.1), when the forcing term is zero ($\beta = 0$), showing bistability between the equilibrium states $u_0 = 0$ and $u_1 = 1$ in an interval enclosed by two transcritical bifurcations, at $\alpha_c = 0$ and $\alpha_c = 1$, respectively. (Online version in colour.)

the bifurcation diagram observed in the LCLV experiment. The average intensity in the feedback loop is plotted against the input laser intensity. For low intensity, the spatial state is a homogeneous one, whereas for increasing input intensity an extended spatio-temporal chaotic state develops, which corresponds to an higher average feedback intensity. In an intermediate

range of intensities, there is a coexistence region where both states can be present. In this region, chaotic localized structures are observed (see the inset of figure 2*a*).

A simple model that contains this type of coexistence and that, at the same time, can be controlled is the Nagumo–Kuramoto model

$$\partial_t u = u(\alpha - u)(u - 1) + \partial_{xx} u + \beta u \cos(kx)[1 + \gamma \psi(x, t)], \tag{3.1}$$

where $u(x, t)$ is a scalar field that describes a bistable forced system, β is the amplitude of the forcing, k the spatial wavenumber, γ the amplitude of the spatio-temporal chaotic source described by the field $\psi(x, t)$ and α rules the relative stability between the trivial stable equilibria of this system, $u_0 = 0$ and $u_1 = 1$ $(0 < \alpha < 1)$. Figure 2*b* shows the bifurcation diagram of the unforced Nagumo–Kuramoto model ($\beta = 0$) as a function of the parameter α. Note that for $\alpha = 0, 1$ the system exhibits transcritical bifurcations and when $\alpha \equiv \alpha_M = \frac{1}{2}$, both states are energetically equivalent, that is, the system is at the Maxwell point [2]. The parameter β, accounting for the intensity of the spatio-temporal forcing, is composed by two parts: a spatial forcing with wavenumber k, and a spatio-temporal chaotic term proportional to γ, generated by the auxiliary spatio-temporal chaotic field $\psi(x, t)$. This field satisfies the following equation:

$$\partial_t \psi = -\psi \partial_x \psi + \epsilon \partial_{xx} \psi - \partial_{xxxx} \psi, \tag{3.2}$$

which corresponds to the well-studied Kuramoto–Sivashinsky model [2,3]. This equation is a prototype model for spatio-temporal chaos [16].

For $\beta = 0$, equation (3.1) describes a simple extended bistable system, *the Nagumo model* [17]. This model was exhaustively studied in the context of population dynamics. In this limit, this model exhibits front propagation between the equilibria [17]. In the case that one considers the spatial forcing, $\beta \neq 0$ and $\gamma = 0$, this term leads the uniform state u_1 to become a spatially periodic one. Note that the forcing term turns into zero for small amplitude of u and then the equilibrium u_0 is unperturbed. Hence, this model has coexistence between a pattern and a uniform state. This type of system is characterized by exhibiting pinning phenomena of the fronts, localized patterns and homoclinic snaking bifurcation diagrams [2,4–6,9].

The inclusion of the term proportional to γ in equation (3.1), which couples the latter equation with equation (3.2), causes the pattern state to exhibit chaotic spatio-temporal behaviours. Moreover, the above model, equation (3.1), presents a coexistence region similar to that displayed by the LCLV experiment. Therefore, one expects the Nagumo–Kuramoto model to show chaoticon states. Figure 3*a* displays a few examples of chaoticon states observed in the LCLV experiment, whereas figure 3*b* shows two examples of the one-dimensional localized spatio-temporal chaotic states exhibited by the Nagumo–Kuramoto model. In figure 3*c*, it is plotted the front interaction ansatz.

All numerical simulations were conducted by using a scheme of finite differences for the space (with up to four neighbours) and a fourth-order Runge–Kutta for time evolution. Specular and periodic boundary conditions were considered in the Nagumo–Kuramoto model equation (3.1) and the Kuramoto–Sivashinsky model equation (3.2), respectively. The simulation length-size was fixed to 512 points with a space discretization $dx = 0.6$ and a time-step $dt = 0.01$ of time evolution.

Each localized structure can be understood as a bound state of two front solutions [7]. In the following section, in order to understand the origin of localized structures exhibited by the Nagumo–Kuramoto model, we study the front dynamics of this model.

(a) Front dynamics

The Nagumo–Kuramoto model equation (3.1) admits a motionless front solution that connects u_0 with u_1 equilibrium, when $\gamma = \beta = 0$ and $\alpha = \alpha_M$. The front has the analytical expression

$$u_{\pm}(x - \delta) = \frac{1}{2} \pm \frac{1}{2} \tanh\left(\frac{\sqrt{2}}{4}(x - \delta)\right), \tag{3.3}$$

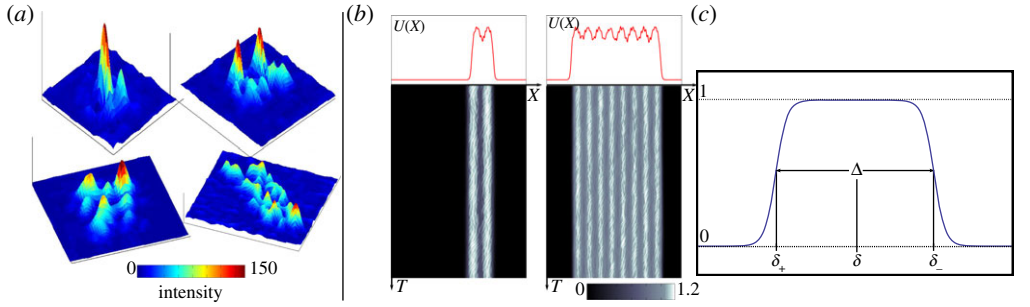

Figure 3. (*a*) Family of localized chaotic structures in the LCLV experiment; intensity surface plots at fixed times. (*b*) Examples of localized chaotic structures in the Nagumo–Kuramoto model, equation (3.1) with $\epsilon = -3, \beta = 0.085, \alpha = -0.14, k = 0.147$ and $\gamma = 0.12$; upper panels: one-dimensional profiles at fixed times; bottom panels: spatio-temporal diagrams with the time series recorded at a time interval $T = 120$. (*c*) Representation of the front interaction ansatz, equation (3.7) for $W = 0$; $\delta_\pm$ are the two front positions, Δ the separation between the two interacting fronts. (Online version in colour.)

where u_+ (u_-) accounts for a monotonous front solution that connects u_0 with u_1 (u_1 with u_0) and δ stands for the position of the front, i.e. the position where the spatial variation of the front is maximum. This particle like solution is parametrized by a symmetry group characterized by the front position δ. Note that the only characteristic length of this solution is the width or core of the front $\kappa = 2\sqrt{2}$, which corresponds to the region where the front has relevant spatial variations close to the front position. To understand the effects of the forcing term and the change of α from the Maxwell point on the front dynamics, we consider $\beta \sim \gamma \ll 1$, $\tilde{\alpha} \equiv \alpha - \frac{1}{2}$ and the following ansatz:

$$u(x,t) = u_+(x - \delta(t)) + W(x,t), \tag{3.4}$$

where the position of the front was promoted to a function of time and W is a small correction function ($W \ll 1$) that account, respectively, for the front dynamics and adjustments of the front solution. Figure 4*a* shows the profile of the front at a given time, when the spatio-temporal forcing is considered. Introducing the above ansatz in equation (3.1) and linearizing in W, we get

$$-\mathcal{L}W = u'_+\dot{\delta} + \tilde{\alpha}u_+(u_+ - 1) + \beta u_+ \cos(kx) + \gamma\beta u_+ \cos(kx)\psi(x,t),$$

where $\mathcal{L} \equiv 3u_+ - 3u_+^2 - \frac{1}{2} + \partial_{xx}$ and u'_+ stands for spatial derivative. Note that u'_+ satisfies $\mathcal{L}u'_+ = 0$ and introducing the inner product $(f|g) = \int_{-\infty}^{\infty} f^*(x)g(x)\,dx$ the linear operator $\mathcal{L}$ is a Sturm–Liouville self-adjoint operator. Hence, to solve the above linear equation, we can apply the solvability condition [2]

$$\dot{\delta}(u'_+|u'_+) + \tilde{\alpha}(u_+^2|u'_+) - \tilde{\alpha}(u_+|u'_+) + \beta(u_+\cos(kx)|u'_+) + \gamma\beta(u_+\cos(kx)\psi(x,t)|u'_+) = 0.$$

Using expression (3.3), and after straightforward calculations, we obtain the kinematic front equation

$$\dot{\delta} = -\frac{\partial U}{\partial \delta} - \gamma\beta(u_+\cos(kx)\psi(x,t)|u'_+), \tag{3.5}$$

with the effective potential

$$U(\delta) \equiv -\frac{\tilde{\alpha}}{2}\delta - \beta\frac{3\pi}{2}\mathrm{csch}(\sqrt{2}k\pi)\sqrt{2+4k^2}\cos\left(k\delta + \arctan\left(\frac{1}{k\sqrt{2}}\right)\right). \tag{3.6}$$

Equation (3.5) gives a description of the front dynamics as a particle type solution. Indeed, the front dynamics can be seen as an overdamped particle trapped into a ratchet potential and urged to move by a chaotic motor, the term proportional to γ. In other words, the position of the front can be interpreted as an overdamped particle in a ratchet potential forcing with a chaotic force. Therefore, the dynamical behaviour of the front position is the deterministic counterpart of a Brownian motor [18]. Figure 4 illustrates the ratchet potential and different trajectories with

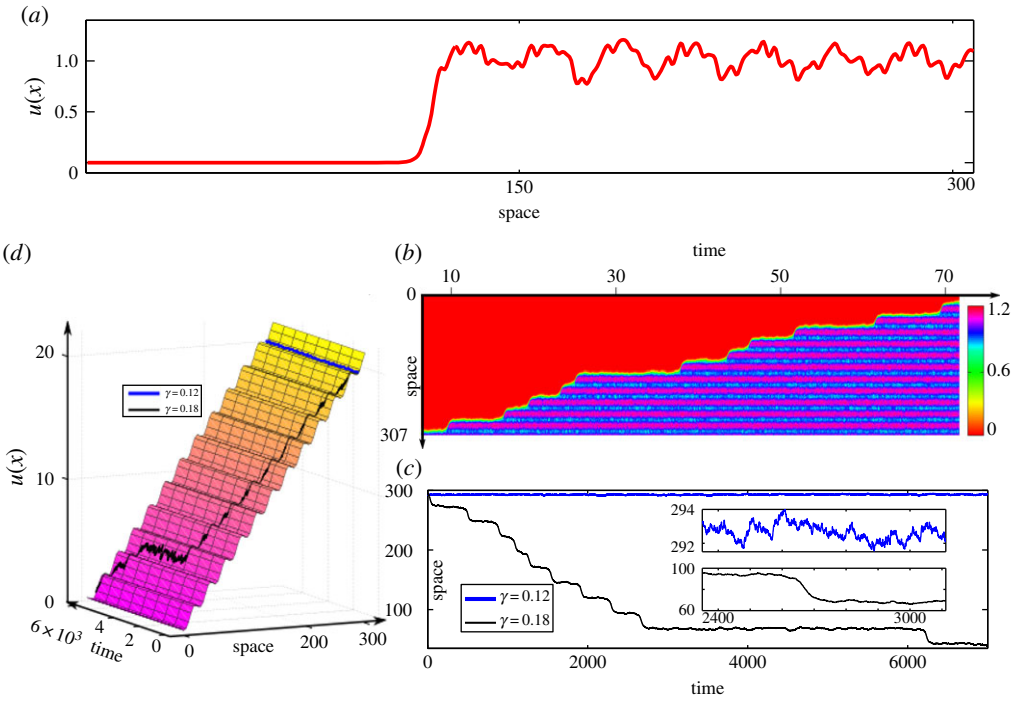

Figure 4. Front propagation between a spatio-temporal chaotic state and a uniform one and *pinning/depinning* transition for the Nagumo–Kuramoto model, equation (3.1), $\epsilon = -3$, $\beta = 0.085$, $\alpha = -0.14$ and $k = 0.147$. (*a*) Front profile $u(x)$ at a given time t. (*b*) Spatio-temporal diagram showing the evolution of the front profile in the depinning region ($\gamma = 0.18$). The pattern endowed with permanent dynamics invades the system. (*c*) Front dynamics in the two regimes : *pinning* (thick line $\gamma = 0.12$) and *depinning* ($\gamma = 0.18$). The inset shows the permanent dynamics at shorter time scale. (*d*) The ratchet potential, expression (3.6), and representation of pinning and depinning trajectories of panel (*c*). (Online version in colour.)

dissimilar values of the intensity of the chaotic forcing. When the intensity of the spatio-temporal forcing γ is small enough, the front position is pinning around a potential minimum and exhibits chaotic oscillations (cf. figure 4*c*,*d*). In opposition, when γ is increased, the front position starts to move in order to minimize the ratchet potential and simultaneously joins with chaotic motions. Figure 4 shows the chaotic front propagation that is characterized by intermittent leaps. Therefore, depending on the value of the intensity of the spatio-temporal forcing γ, the front experiences a *pinning/depinning* transition. In brief, the dynamics of the position of the front is described by a chaotic motor.

(b) Chaoticon as interaction of fronts

To study the existence, stability properties, dynamical evolution and bifurcation diagram of the spatio-temporal localized structures, we can consider this state as a bound state of two fronts [7,9]. Indeed, these localized states can be understood as solutions composed of two fundamental states, the front solutions. It is worthy to note that localized states are not always considered as bound states of two fronts. However, in some limit of the parameters, these states can be satisfactorily described as bound states. A paradigmatic example of this property is the pulse solutions observed in the cubic quintic Ginzburg–Landau equation [12]. This pulse solution can be understood as a bound state of two fronts in the perturbed dissipative limit of the Ginzburg–Landau equation [19]. In general, close to the Maxwell point, the localized structures can be well described in terms of front interaction.

Let us consider—close to the Maxwell point and for small spatio-temporal forcing, $\beta \sim \gamma \sim \tilde{\alpha} \ll 1$—the following ansatz for the front interaction

$$u(x,t) = [u_+(x-\delta_+(t)) + u_-(x-\delta_-(t)) - u_1] + W(x,t), \tag{3.7}$$

where $W(x,t)$ is a small correction function ($W \ll 1$). This ansatz is composed by two fronts positioned at $\delta_+(t)$ and $\delta_-(t)$, respectively, with $\delta_+(t) < \delta_-(t)$ and a reference constant state u_1. Figure 3*c* illustrates the above ansatz when $W = 0$. Note that the position (δ) and the width (Δ) of this localized state are given by

$$\left.\begin{aligned} \delta(t) &\equiv \frac{\delta_+(t) + \delta_-(t)}{2} \\ \text{and} \qquad \hat{\Delta}(t) &\equiv \delta_-(t) - \delta_+(t). \end{aligned}\right\} \tag{3.8}$$

For the sake of simplicity, we renormalize the width of the localized structure in units of the core front, $\Delta(t) = \hat{\Delta}(t)/\kappa$. It must be pointed out that the above ansatz, equation (3.7), is invariant under the change $u_+ \leftrightarrow u_-$. Introducing this ansatz into (3.1), linearizing in W and neglecting any product of W with the perturbative parameters (γ, β, and α), after straightforward calculations we obtain

$$\begin{aligned} \mathcal{L}_\pm W = &-3(u_\mp - 1)(1 - u_\pm)[(u_\mp - 1) + u_\pm] \\ &- \alpha[u_\pm + (u_\mp - 1)][(u_\pm - 1) + (u_\mp - 1)] \\ &- \beta[u_\pm + (u_\mp - 1)]\cos(kx)(1 + \gamma\psi) + \dot{\delta}_\mp u'_\mp + \dot{\delta}_\pm u'_\pm \end{aligned} \tag{3.9}$$

with

$$\mathcal{L}_\pm = [-3u_\pm + 3u_\pm^2 + \tfrac{1}{2} - \partial_{xx}] - 3(u_\mp - 1)[-1 + 2u_\pm + (u_\mp - 1)].$$

This operator can be written as $\mathcal{L}_\pm = \mathcal{L}^{(\pm)} + \mathcal{L}_I$, where

$$\mathcal{L}^{(\pm)} \equiv [-3u_\pm + 3u_\pm^2 + \tfrac{1}{2} - \partial_{xx}]$$

is the same operator that characterizes the dynamics of a front $u_\pm$ (cf. §3*a*) and

$$\mathcal{L}_I \equiv -3(u_\mp - 1)[-1 + 2u_\pm + (u_\mp - 1)].$$

As a consequence of the invariance $u_+ \leftrightarrow u_-$, the linear equation for W can be written in two similar ways, this is the origin of $\pm$ sign in equation (3.9). In order to compute the front dynamics of one of the two fronts, it is useful to consider one of the respective signs.

Analogously to the procedure adopted in the section on front dynamics (cf. §3*a*), in order to solve linear equation (3.9), we have to apply the solvability condition. Indeed, to apply the solvability condition, we must characterize the *kernel* of the adjoint operator of $\mathcal{L}_\pm$. Thus, we consider the same inner product of the previous section, where $\mathcal{L}_\pm$ is self-adjoint. Owing to $\mathcal{L}^{(\pm)}u'_\pm = 0$, one has to calculate the *kernel* of $\mathcal{L}_I$ in order to characterize the *kernel* of $\mathcal{L}_\pm$. In spite that $\mathcal{L}_I u'_\pm \neq 0$, if we assume that the distance between the two fronts is large enough ($|\delta_+ - \delta_-| \gg 1$, diluted fronts), then $\mathcal{L}_I u'_\pm \approx \exp(-\kappa(\delta_- - \delta_+))$, where $\kappa = 2\sqrt{2}$ is the core of the front. This operator $\mathcal{L}_I$ accounts for the interaction of one front with the other. More precisely, this operator accounts for the asymptotic value of $u_\pm - u_1$ around the other front $u_\mp$, which is exponentially small [$\exp(-\kappa(\delta_- - \delta_+))$]. Note that any term of the form $(u'_\pm|(u_\pm - 1)^{n>1})$ is exponentially small in the limit of diluted fronts.

Applying the solvability conditions in equation (3.9), we obtain the following two equations:

$$\begin{aligned} 0 = &[(3 + 2\alpha)(u_\pm u_\mp|u'_\pm) - 3(u_\mp u_\pm^2|u'_\pm) - \alpha(u_\mp|u'_\pm) + \beta(u_\mp\cos(kx)|u'_\pm) \\ &+ \beta\gamma(u_\mp\cos(kx)\psi|u'_\pm) + \dot{\delta}_\mp(u'_\mp|u'_\pm)] + [(u_\pm^2|u_\pm)(3 + \alpha) - 3(1 + \alpha)(u_\pm|u'_\pm) \\ &+ \alpha(1|u'_\pm) + \beta(u_\pm\cos(kx)|u'_\pm) + \beta\gamma(u_\pm\cos(kx)\psi|u'_\pm) - \beta(\cos(kx)|u'_\pm) \\ &- \beta\gamma(\cos(kx)\psi|u'_\pm) + \dot{\delta}_\pm(u'_\pm|u'_\pm)]. \end{aligned}$$

To simplify the above expressions and to grasp the front interaction, we consider the diluted limit, i.e. we contemplate that the distance between the fronts is large enough in comparison to the core of the front ($\Delta \gg \kappa = 2\sqrt{2}$). It is important to note that in the above expressions we have two kinds of integrals, *interaction terms* $[(f(u_\pm)|g(u_\mp)]$ and *non-interaction terms* $[(f(u_\pm)|g(u_\pm)]$. The non-interaction terms can be calculated analytically and the interaction terms can be calculated at the dominant order, that is, we consider only the exponential interaction, which is a consequence of the effect of the tail of one front over the other front. In order to accomplish this calculations, we split the integral in two regions

$$(f(u_+)|u'_-) = \int_{-\infty}^{\infty} f(u_+)u'_- = \int_{-\infty}^{\delta} f(u_+)\check{u}'_- + \int_{\delta}^{\infty} f(\check{u}_+)u'_- = I + II.$$

In the integration interval of the first integral I, $x = \delta_-$ is not present. Thus, we can approximate u'_- by its asymptotic expression far from the core of the front around to the other front $-\sqrt{2}\,\mathrm{e}^{-\sqrt{2}\Delta(t)/4}/8$ (denoted by $\check{u}'_-$). We use the same type of asymptotic approximation for the second integral II and all the *interaction terms*. After straightforward calculations, the set of equations for the centre of mass δ and the size of the localized structure Δ are [20]

$$\dot{\delta} = -\frac{3\beta}{4\sqrt{2}} C_3(\Delta)\sin(k\delta + \phi_3(\Delta)) - \frac{3\beta\gamma}{4\sqrt{2}}(\psi[u_+ + u_- - 1]\cos(kx)|u'_+ + u'_-) \tag{3.10}$$

and

$$\begin{aligned}\dot{\Delta} = &\left(\frac{15}{32}\sqrt{2} + \frac{9}{4}\right)\mathrm{e}^{-\sqrt{2}\Delta/4} - \tilde{\alpha}\frac{\sqrt{2}}{4} + \frac{3}{8}\beta G_3(\delta)\sin\left(\frac{4k\Delta}{\sqrt{2}} + \theta_3(\delta)\right)\\ &+ \frac{3}{8}\beta\gamma((u_- + u_+ - 1)\psi\cos(kx)|u'_+ - u'_-),\end{aligned} \tag{3.11}$$

where

$$C_3 = \sqrt{C_1^2\sin^2\left(\frac{4k\Delta}{\sqrt{2}} + \phi_1\right) + C_2^2\sin^2\left(\frac{4k\Delta}{\sqrt{2}} + \phi_2\right)},$$

$$\phi_3 = \arctan\left(\frac{C_2\sin(4k\Delta/\sqrt{2} + \phi_2)}{C_1\sin(4k\Delta/\sqrt{2} + \phi_1)}\right),$$

$$C_2 = \sqrt{(A_+ + A_-)^2 + (B_+ - B_-)^2}, \quad \phi_2 = \arctan\left(\frac{B_+ - B_-}{A_+ + A_-}\right),$$

$$C_1 = \sqrt{(12k\pi\,\mathrm{csch}(\sqrt{2}k\pi) + A_+ + A_-)^2 + (4\sqrt{2}k^2\pi\,\mathrm{csch}(\sqrt{2}k\pi) - B_- - B_+)^2}$$

$$\phi_1 = \arctan\left(\frac{2k\pi\,\mathrm{csch}(\sqrt{2}k\pi) + A_+ + A_-}{B_- + B_- 4\sqrt{2}k\pi\,\mathrm{csch}(\sqrt{2}k\pi)}\right),$$

$$G_3 = \sqrt{G_1^2\sin^2(k\delta + \theta_1) + G_2^2\sin^2(k\delta + \theta_2)}, \quad \theta_3 = \arctan\left(\frac{G_2\sin(4k\delta + \theta_2)}{G_1\sin(4k\delta + \theta_1)}\right),$$

$$G_2 = \sqrt{(A_+ + A_-)^2 + (4\sqrt{2}k^2\pi\,\mathrm{csch}(\sqrt{2}k\pi) - B_+ - B_-)^2},$$

$$\theta_2 = \arctan\left(\frac{-(A_+ + A_-)}{4\sqrt{2}k^2\pi\,\mathrm{csch}(\sqrt{2}k\pi) - B_+ - B_-}\right),$$

$$G_1 = \sqrt{(-4k\pi\,\mathrm{csch}(\sqrt{2}k\pi) - A_+ + A_-)^2 + (B_+ - B_-)^2},$$

$$\theta_1 = \arctan\left(\frac{B_+ - B_-}{-4k\pi\,\mathrm{csch}(\sqrt{2}k\pi) - A_+ + A_-}\right),$$

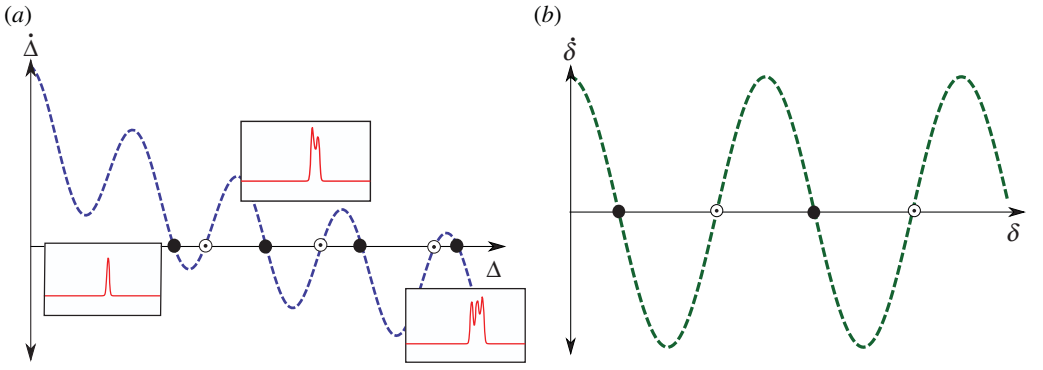

Figure 5. Phase portraits of (*a*) the size of the localized structure Δ and (*b*) the centre of mass δ when $\beta = 1, \gamma = 0, \alpha = 4.7$, $k = 6.62$, $C_3 = 1.5$ and $G_3 = 1.5$. The filled and empty circles are stable and unstable equilibria, respectively. The insets in (*a*) are numerical plots of the predicted localized solutions. (Online version in colour.)

$$A_{\pm} = \sqrt{2}\int_{-\infty}^{\infty} (\pm 1 - \tanh(z))\,\mathrm{sech}^2(z \mp \Delta)\cos(2\sqrt{2}kz)\,\mathrm{d}z$$

and

$$B_{\pm} = \sqrt{2}\int_{-\infty}^{\infty} (\pm 1 - \tanh(z))\,\mathrm{sech}^2(z \mp \Delta)\sin(2\sqrt{2}kz)\,\mathrm{d}z.$$

Equation (3.10) describes the dynamics of the position of the localized states, which corresponds to a kinematic equation composed by two forces: a periodic force, due to the spatial forcing, and a chaotic force accounting for the chaotic forcing, which are proportional to β and γ, respectively. Note that the expression $(\psi(x,t)[u_+ + u_- - 1]\cos(kx)|u'_+ + u'_-)$ accounts for a temporal chaotic force. To figure out the dynamics of the position of the localized states, we can neglect the chaotic forcing ($\beta \gg \gamma$). Thus, the centre of mass of the localized state satisfies the equation of an overdamped particle under a periodic potential with a wavenumber k and a magnitude proportional to β. Figure 5*a* displays the phase portrait of the size Δ of the localized structures, whereas figure 5*b* shows the phase portraits of the centre of mass δ of the localized states. The centres of mass will be positioned in specific positions induced by the spatial forcing, which are emphasized by points in figure 5*b*. The filled (empty) points stand for stable (unstable) centre of mass position. The inclusion of spatio-temporal forcing ($\gamma \lesssim \beta$) induces small aperiodic fluctuations around the equilibria position of the centre of mass (cf. figure 3*b*).

On the other hand, equation (3.10) describes the dynamics of the width of the localized state, which corresponds to a kinematic equation composed by four forces. The first one is proportional to $\mathrm{e}^{-\sqrt{2}\Delta/4}$ and accounts for the interaction of fronts. This force is exponentially small in the limit of dilute fronts [21]. The second term is proportional to $\tilde{\alpha}$ and accounts for the energy difference between the two uniform equilibria. This term vanishes at the Maxwell point. The balance between the interaction of fronts and the energy difference may generate unstable localized structures [7]. The last two terms in equation (3.10) account for a periodic and chaotic force, respectively, corresponding to the spatial and spatio-temporal chaotic forcing that are proportional to β and γ, respectively. In order to understand the underlying dynamics of this equation, we first neglect the effects of the spatio-temporal forcing ($\gamma \ll 1$). In this limit, equation (3.10) describes the interaction between a pattern and a homogeneous state. The force in this limit is shown in figure 5*a*.

As a result of the combination of the interaction of fronts and of the spatial forcing, the system exhibits a family of localized patterns [9] (cf. inset of figure 5*a*). Modifying the parameter α, the localized states appear and disappear by a cascade of saddle-node bifurcations, giving rise to a complex phase diagram called the homoclinic snaking bifurcation [22]. Recently, this type of snaking bifurcation has been verified experimentally in an LCLV with a spatially modulated

optical feedback [23]. The inclusion of a small spatio-temporal forcing leads the pattern state to become a spatio-temporal chaotic one, then, localized patterns turn into localized spatio-temporal chaotic states, *chaoticons*. Therefore, the holding mechanism of localized spatio-temporal chaotic states is induced by the pinning generated by the spatio-temporal forcing, by means of the nucleation barrier that blocks the motion of the fronts. This mechanism prevents that aperiodic fluctuations cross the nucleation barrier. Then, chaoticons have a width that aperiodically fluctuates around a value which is of the order of some wavelengths. When γ is increased the fronts begin to propagate, as it is illustrated in figure 4, consequently chaoticons are unstable. For small γ, as a result of the interaction law (3.10) the system exhibits a family of chaoticons with different sizes (figure 5*a*). From this kinematic law, one concludes that chaoticons appear and disappear through saddle-node bifurcations. The corresponding snaking bifurcation diagram of chaoticons is an open problem, since from the geometrical point of view the dynamics of the manifold associated with chaotic states is not understood yet [24].

4. Conclusion and comment

Localized states with a complex spatio-temporal dynamics are observed in physical systems that exhibit coexistence between a chaotic spatio-temporal pattern and a uniform state. This coexistence is the essential ingredient to observe these localized states. We have established analytically a holding mechanism of localized spatio-temporal chaotic state in one-dimensional extended systems. This mechanism is based on the spatio-temporal chaotic pattern that induces a nucleation barrier to the motion of the fronts connecting the pattern with another state. This finding is derived in the context of the Nagumo–Kuramoto model, equation (3.1), which exhibits localized spatio-temporal chaotic states. However, the established mechanism applies beyond the mastery of this simple model. Therefore, in any system which exhibits coexistence of chaotic spatio-temporal patterns and other states one expects domains between these states to exhibit pinning phenomena. In model (3.1), the pinning is induced by the spatial forcing, notwithstanding in the LCLV experiment with optical feedback the spatio-temporal complexity self-induces this pinning phenomenon. The advantage of model (3.1) from the theoretical point of view is that one can control the characteristic intensity of the spatio-temporal chaos. This model allows us to unveil the front dynamics, which is characterized by a chaotic motor, and the front interaction mechanism at the origin of the localized spatio-temporal chaotic structures. Experimentally, it is a complicated task to control the amplitude of the aperiodic oscillations.

In the context of discrete coupled oscillators, localized states that separate a coherent and phase locked domain with an incoherent and desynchronized one have been observed [25]. These intriguing states, denominated *chimera states*, can be understood as the counterpart of the chaoticon states in discrete systems. It is known that the effect of spatial discretization is analogous to a spacial forcing in the continuous limit. Therefore, the discretization can be responsible for the pinning mechanism of localized states [26].

In conclusion, we have shown that the mechanism responsible for the existence of chaoticons is the pinning and interaction of the fronts, which is induced by a chaotic spatio-temporal structure. Hence, we can conjecture that a system with coexistence of spatio-temporal chaos and a periodic structure will present similar chaoticon states. Works in this direction are in progress.

Funding statement. We acknowledge financial support of the ANR international program, project ANR-2010-INTB-402-02 (ANR-CONICYT39), 'COLORS'. M.G.C. thanks financial support of FONDECYT project 1120320. N.V. thanks the Master fellowship from CONICYT contract 22111114 and financial support of DPP of the University of Chile.

References

1. Nicolis G, Prigogine I. 1997 *Self-organization in non equilibrium systems*. New York, NY: John Wiley & Sons.

2. Pismen LM. 2006 *Patterns and interfaces in dissipative dynamics*. Springer Series in Synergetics. Berlin, Germany Springer.
3. Cross MC, Hohenberg PC. 1993 Pattern formation outside of equilibrium. *Rev. Mod. Phys.* **65**, 851–1112. (doi:10.1103/RevModPhys.65.851)
4. Descalzi O, Clerc M, Residori S, Assanto G (eds). 2010 *Localized states in physics: solitons and patterns*. Berlin, Germany: Springer.
5. Purwins HG, Bodeker HU, Amiranashvili Sh. 2010 Dissipative solitons. *Adv. Phys.* **59**, 485–701. (doi:10.1080/00018732.2010.498228)
6. Ackemann T, Firth WJ, Oppo GL. 2009 Fundamentals and applications of spatial dissipative solitons in photonic devices. In *Advances in atomic, molecular, and optical physics*, vol. 57 (eds E Arimondo, PR Berman, CC Lin), pp. 323–421. Burlington, VT: Academic Press.
7. Coullet P. 2002 Localized patterns and fronts in nonequilibrium systems. *Int. J. Bifurc. Chaos* **12**, 2445. (doi:10.1142/S021812740200614X)
8. Tlidi M, Mandel P, Lefever R. 1994 Localized structures and localized patterns in optical bistability. *Phys. Rev. Lett.* **73**, 640. (doi:10.1103/PhysRevLett.73.640)
9. Clerc MG, Falcon C. 2005 Localized patterns and hole solutions in one-dimensional extended systems. *Physica A* **356**, 48–53. (doi:10.1016/j.physa.2005.05.011)
10. Bortolozzo U, Clerc MG, Falcon C, Residori S, Rojas R. 2006 Localized states in bistable pattern forming systems. *Phys. Rev. Lett.* **96**, 214501. (doi:10.1103/PhysRevLett.96.214501)
11. Barashenkov IV, Zemlyanaya EV, van Heerden TC. 2011 Time-periodic solitons in a damped-driven nonlinear Schrodinger equation. *Phys. Rev.* **E83**, 056609. (doi:10.1103/PhysRevE.83.056609)
12. Fauve S, Thual O. 1990 Solitary waves generated by subcritical instabilities in dissipative systems. *Phys. Rev. Lett.* **64**, 282–284. (doi:10.1103/PhysRevLett.64.282)
13. Clerc MG, Coulibaly S, Laroze D. 2012 Localized waves in a parametrically driven magnetic nanowire. *Eur Phys. Lett.* **97**, 30006. (doi:10.1209/0295-5075/97/30006)
14. Verschueren N, Bortolozzo U, Clerc MG, Residori S. 2013 Spatiotemporal chaotic localized state in liquid crystal light valve experiments with optical feedback. *Phys. Rev. Lett.* **110**, 104101. (doi:10.1103/PhysRevLett.110.104101)
15. Residori S. 2005 Patterns, fronts and structures in a liquid-crystal-light-valve with optical feedback. *Phys. Rep.* **416**, 201–272. (doi:10.1016/j.physrep.2005.06.004)
16. Kuramoto Y. 1984 *Chemical oscillations, waves, and turbulence*. New York, NY: Springer.
17. Murray JD. 1989 *Mathematical biology*. Berlin, Germany: Springer.
18. Reimann P, Hanggi P. 2002 Introduction to the physics of Brownian motors. *Appl. Phys. A* **75**, 169–178. (doi:10.1007/s003390201331)
19. Hakim VV, Pomeau Y. 1991 On stable localized structures and subcritical instabilities. *Eur. J. Mech. B/Fluids* **10**, 137–143.
20. Verschueren N. 2013 Fenómenos no variacionales en patrones. M.Sc. thesis, University of Chile. See http://www.tesis.uchile.cl/handle/2250/114076.
21. Kawasaki K, Otha T. 1982 Kink dynamics in one-dimensional nonlinear systems. *Physica A* **116**, 573–593. (doidoi:10.1016/0378-4371(82)90178-9)
22. Woods PD, Champneys AR. 1999 Heteroclinic tangles and homoclinic snaking in the unfolding of a degenerate reversible Hamiltonian-Hopf bifurcation. *Physica D* **129**, 147–170. (doi:10.1016/S0167-2789(98)00309-1)
23. Haudin F, Rojas RG, Bortolozzo U, Residori S, Clerc MG. 2011 Homoclinic snaking of localized patterns in a spatially forced system. *Phys. Rev. Lett.* **107**, 264101. (doi:10.1103/PhysRevLett.107.264101)
24. Wiggins S. 1994 *Normally hyperbolic invariant manifolds in dynamical systems*. New York, NY: Springer.
25. Abrams D, Strogatz S. 2004 Chimera states for coupled oscillators. *Phys. Rev. Lett.* **93**, 174102. (doi:10.1103/PhysRevLett.93.174102)
26. Clerc MG, Elías RG, Rojas RG. 2010 Continuous description of lattice discreteness effects in front propagation. *Phil. Trans. R. Soc. A* **369**, 412–424. (doi:10.1098/rsta.2010.0255)